Demonstration of ITER operational scenarios on DIII-D

2010 Nucl. Fusion 50 075005

(http://iopscience.iop.org/0029-5515/50/7/075005)

IOP Publishing and International Atomic Energy Agency Nuclear Fusion

Nucl. Fusion **50** (2010) 075005 (8pp) doi:10.1088/0029-5515/50/7/075005

Demonstration of ITER operational scenarios on DIII-D*

E.J. Doyle[1,9], J.C. DeBoo[2], J.R. Ferron[2], G.L. Jackson[2], T.C. Luce[2], M. Murakami[3], T.H. Osborne[2], J.-M. Park[3], P.A. Politzer[2], H. Reimerdes[4], R.V. Budny[5], T.A. Casper[6], C.D. Challis[7], R.J. Groebner[2], C.T. Holcomb[6], A.W. Hyatt[2], R.J. La Haye[2], G.R. McKee[8], T.W. Petrie[2], C.C. Petty[2], T.L. Rhodes[1], M.W. Shafer[8], P.B. Snyder[2], E.J. Strait[2], M.R. Wade[2], G. Wang[1], W.P. West[2,10] and L. Zeng[1]

[1] Department of Physics and Astronomy, and PSTI, University of California, Los Angeles, CA 90095, USA
[2] General Atomics, PO Box 85608, San Diego, CA 92186-5608, USA
[3] Oak Ridge National Laboratory, Oak Ridge, TN, USA
[4] Department of Applied Physics and Applied Mathematics, Columbia University, New York, NY, USA
[5] Princeton Plasma Physics Laboratory, Princeton, NJ, USA
[6] Lawrence Livermore National Laboratory, Livermore, CA, USA
[7] Euratom/CCFE Fusion Association, Culham Science Centre, Oxon OX14 3DB, UK
[8] Department of Energy Physics, University of Wisconsin-Madison, Madison, WI, USA

E-mail: edoyle@ucla.edu

Received 6 January 2010, accepted for publication 17 May 2010
Published 8 June 2010
Online at stacks.iop.org/NF/50/075005

Abstract
The DIII-D programme has recently initiated an effort to provide suitably scaled experimental evaluations of four primary ITER operational scenarios. New and unique features of this work are that the plasmas incorporate essential features of the ITER scenarios and anticipated operating characteristics; e.g. the plasma cross-section, aspect ratio and value of I/aB of the DIII-D discharges match the ITER design, with size reduced by a factor of 3.7. Key aspects of all four scenarios, such as target values for β_N and H_{98}, have been replicated successfully on DIII-D, providing an improved and unified physics basis for transport and stability modelling, as well as for performance extrapolation to ITER. In all four scenarios, normalized performance equals or closely approaches that required to realize the physics and technology goals of ITER, and projections of the DIII-D discharges are consistent with ITER achieving its goals of $\geqslant$400 MW of fusion power production and $Q \geqslant 10$. These studies also address many of the key physics issues related to the ITER design, including the L–H transition power threshold, the size of edge localized modes, pedestal parameter scaling, the impact of tearing modes on confinement and disruptivity, beta limits and the required capabilities of the plasma control system. An example of direct influence on the ITER design from this work is a modification of the physics requirements for the poloidal field coil set at 15 MA, based on observations that the inductance in the baseline scenario case evolves to a value that lies outside the original ITER specification.

PACS numbers: 52.55.Fa, 52.55.−s, 28.52.−s

(Some figures in this article are in colour only in the electronic version)

1. Introduction

It is critical to the future success of US and worldwide fusion programmes that the ITER tokamak [1] meets its physics and technology goals. The expected performance of ITER can be investigated on present devices via experiments which match absolute or normalized ITER plasma parameters, e.g. [2–7]. Towards this end, the DIII-D programme recently initiated an effort to provide suitably scaled experimental evaluations of four primary ITER operational scenarios. New and unique features of this work are that the plasmas incorporate essential operational features of the ITER scenarios, such as the design

* Presented at the *22nd IAEA Fusion Energy Conf. (Geneva, Switzerland, 13–18 October 2008)* http://www-pub.iaea.org/MTCD/Meetings/fec2008pp.asp

[9] Author to whom any correspondence should be addressed.

[10] Deceased.

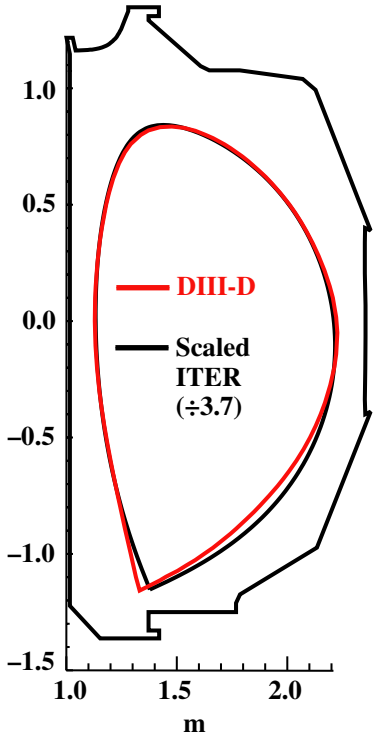

Figure 1. Comparison of scaled (reduced by factor of 3.7) ITER plasma cross-section (black) and experimental DIII-D plasma cross-section (red/grey). (Colour online.)

shape of the ITER plasma cross-section and the design value for the aspect ratio. Evaluation of the four ITER scenarios on a single tokamak enables direct cross-comparisons of performance and operational issues. The four ITER scenarios [1, 7] which have been demonstrated are the baseline or reference scenario, which targets a fusion gain factor (Q) of 10 using a conventional ELMing H-mode discharge at 15 MA plasma current; the hybrid scenario, which targets a high neutron fluence mission at reduced plasma current (∼12 MA), operating with enhanced stability; the steady-state scenario, which seeks fully noninductive (NI) operation at lower plasma currents (∼9 MA), employing enhanced confinement and stability in order to obtain a target $Q \sim 5$ and the 'advanced inductive' (AI) scenario, which targets ITER's goals of investigating ignited or near-ignited plasmas ($Q \geqslant 20$) and 700 MW fusion power output, by combining full current operation with the increased plasma stability limits characteristic of hybrid operation. Key aspects of all four of these scenarios have been replicated successfully on DIII-D, providing an improved and unified physics basis for transport and stability modelling, as well as performance extrapolation to ITER. In all four scenarios, performance equals or closely approaches that required to realize the physics and technology goals of ITER.

That plasma shaping plays a significant role in determining plasma stability limits, confinement and pedestal properties is well understood [8–10], and both modelling and experiment indicate that the edge plasma stability is sensitive to small variations in plasma shape [11]. Consequently, all four scenarios were operated on DIII-D with a version of the ITER plasma scaled by a factor of 3.7, as shown in figure 1. This choice of scale factor allowed us to simultaneously meet four constraints: (1) matching the shape of the ITER plasma cross-section within the DIII-D vacuum vessel, (2) matching the ITER design aspect ratio of 3.1, (3) providing a pumping capability for these discharges using the lower, outer cryopump on DIII-D and (4) providing a relatively large outer gap for steady-state plasma operation. Operating with the correct ITER plasma cross-section and aspect ratio is a unique feature of this work. These demonstrations focus on the current flat-top phase of the discharges; in general no attempt was made to simulate ITER startup prescriptions and constraints, which were addressed in separate work [12, 13]. The demonstration discharges were operated with predominant co-NBI, driving significant plasma toroidal rotation which is known to affect confinement, e.g. [10, 14]. In addition, not all of the scenarios were operated with $T_i = T_e$, as anticipated on ITER. These issues, and others such as shape sensitivity studies, will be addressed in future work.

The rest of this paper is structured as follows. Section 2 presents an overview or summary of the results achieved for the four scenarios on DIII-D in tabular form and also outlines how performance projections to ITER have been made. Results from the baseline, steady-state, hybrid and AI scenario are then presented in sections 3–6, respectively. Section 7 discusses key ITER physics issues addressed by the DIII-D demonstration discharges, while section 8 presents conclusions from this work.

2. Overview of DIII-D realizations of ITER operating scenarios and projections to ITER

The basic parameters obtained for the four ITER scenarios evaluated on DIII-D are presented here. Apart from the ITER-like startup variant of the hybrid scenario, all plasmas were run at a common magnetic field of 1.9 T, in order to facilitate direct comparisons on DIII-D and to anticipated operating scenarios at fixed (full) field on ITER. Projections of the DIII-D results to fusion power output (P_{fus}) and Q on ITER are made using a spreadsheet model which implements the methodology described in [4]. The projections to ITER are made for the same β_N as achieved on DIII-D, using the DIII-D electron temperature profile and with $T_i = T_e$, but with the density profile scaled to give $n_e = 0.85\, n_G$, where $n_G \equiv I/\pi a^2$ (10^{20} m^{-3}, MA, m) is the Greenwald density. Three different confinement scalings are used in making the projections: the L-mode ITER-89P scaling (confinement scaling factor denoted by H_{89}) [15], which is Bohm-like; a pure gyroBohm (DS03) scaling derived from the ITER database [16] and the ITER H-mode scaling, IPB98y2 (confinement factor denoted by H_{98}) [17], which has an intermediate character between Bohm and gyroBohm. These projections and the plasma parameters achieved for the four scenarios described in the following sections are summarized in table 1

3. ITER baseline scenario

Conventional ELMy H-mode plasmas have been operated at a normalized current $I_N \equiv I/aB$ (MA, m, T) value of 1.415, corresponding to 15 MA operation on ITER. Use of I_N allows a definite translation of plasma current from ITER to DIII-D,

Table 1. Parameters at full performance for the four operating scenarios.

	Baseline (131498)	Hybrid DIII-D startup (131711)	Hybrid ITER startup (131265)	Advanced inductive (133137)	Steady state (131198)
β_N, β_p	1.8, 0.65	2.2, 1.1	2.8, 1.3	2.8, 1.05	3.0, 1.6
Equivalent ITER I_p (MA)	15.0	11.4	11.2	14.8	10.7
q_{95}	3.1	4.3	4.1	3.3	4.7
H_{89}, H_{98}	2.0, 1.1	2.6, 1.5	2.5, 1.45	2.4, 1.5	2.2, 1.46
G	0.37	0.31	0.4	0.6	0.3
B (T), I_p (MA)	1.92, 1.47	1.92, 1.13	2.11, 1.28	1.93, 1.49	1.92, 1.05
n (10^{19} m^{-3}), n/n_G	8–10, 0.5–0.65	6.6, 0.55	5.3, 0.41	5.3, 0.35	4.7, 0.4
P_{aux} (MW)	3.5	3.47	8.0	7.7	9.38
τ_E (s)	0.22	0.24	0.17	0.18	0.115
$v_\phi(0)$ (km s^{-1}), M_ϕ	140, 0.26	220, 0.4	290, 0.36	220, 0.3	190, 0.4
$\langle p \rangle \tau_E$ (kPa s)	8.1	8.4	9.7	10.4	5.3
Z_{eff}	3.0	2.9	1.9	1.8	1.9
Averaging time (s)	2.6–3.6	2.85–3.45	2.8–3.3	2.8–3.8	3.4–3.9
P_{fus} (MW) (89P, 98y2, DS03)	443, 427, 404	382, 371, 329	532, 477, 432	818, 723, 723	532, 502, 452
Q (Projected to ITER) (89P, 98y2, DS03)	10.3, 22.4, ∞	6.3, 10.2, ∞	5.8, 23.3, ∞	13.5, ∞, ∞	2.7, 5.8, 19.8
Auxiliary heating	NBI	NBI	NBI	NBI	NBI + off-axis ECCD
Internal MHD	Sawteeth, $n = 2$ tearing	Sawteeth, $n = 2$ tearing	Fishbones, $n = 3$ tearing	Sawteeth, $n = 3$ tearing	$n = 3$ tearing

given the same plasma shape. The resulting value of the safety factor at the 95% flux surface (q_{95}) is 3.1, close to the ITER design value of 3.0. The plasma was operated with feedback control of the NBI power so as to maintain the ITER target value of normalized beta, $\beta_N = 1.8$. The time evolution of the main plasma parameters for such a discharge is illustrated in figure 2, while profiles are shown in figure 3. As can be seen (figure 2(*b*)), confinement is at or above the ITER target of $H_{98} = 1.0$, while the density (figure 2(*d*)) increases up to the absolute density of 1.0×10^{20} m^{-3} anticipated for ITER, which is $\sim 0.65 n_G$ on DIII-D. Tearing modes are present and decrease confinement by $\sim$10%. Due to the high operating density, beyond the cutoff density for 110 GHz gyrotron sources, no attempt was made to mitigate the effects of these modes by application of electron cyclotron current drive (ECCD). As shown in (figure 2(*c*)), the parameter $G \equiv \beta_N H_{89}/q_{95}^2$ [4], a measure of the normalized fusion performance, is close to the 0.42 level predicted for $Q = 10$ operation on ITER (much of the difference is due to the fact that q_{95} is not 3.0, as originally assumed for ITER). As shown in table 1, however, the more detailed spreadsheet model projects that this discharge meets or exceeds the ITER targets of 400 MW of fusion power and $Q \geqslant 10$ for this scenario, for all three confinement scalings utilized.

Two other major features of these discharges are also evident in figure 2. The baseline discharges exhibit large and infrequent (<10 Hz) type I ELMs, leading to poor density and impurity control. The ELM and pedestal characteristics of these discharges are of considerable interest and are described in more detail in a separate section below (section 7). In many of these discharges, ELMs are observed to trigger 2/1 NTM activity, leading to plasma termination. The NTM activity in these discharges and prospects for stabilization using localized ECCD are discussed in detail in [18]. The 3 s H-mode period in these discharges corresponds to $\sim 3\tau_R$, or approximately the same normalized duration as anticipated for ITER. However, the discharges are non-stationary, as is evident in the increase in density and modest decline in confinement with time (figure 2), and also in the fact that the plasma internal inductance continually declines during the H-mode period (not shown).

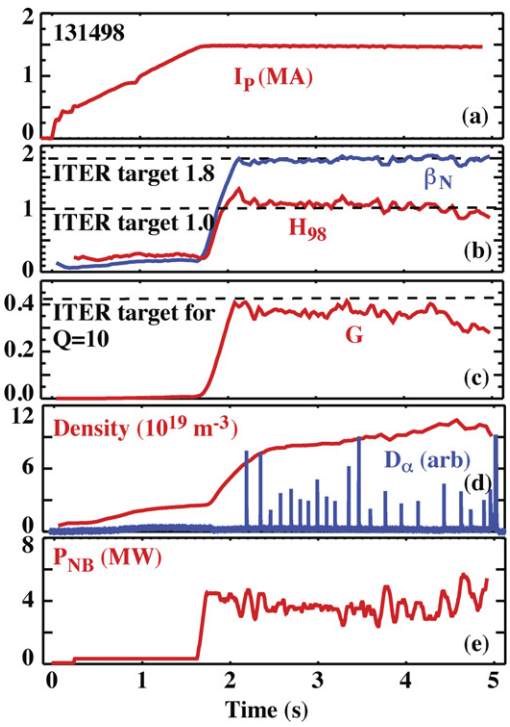

Figure 2. Time evolution of key plasma parameters for a baseline scenario demonstration discharge, operating at a normalized plasma current equivalent to 15 MA on ITER (131498). Illustrated are (*a*) plasma current I_p; (*b*) normalized beta β_N and confinement factor H_{98}, with ITER target values; (*c*) fusion performance factor $G \equiv \beta_N H_{89}/q_{95}^2$, with target value for $Q = 10$ operation on ITER indicated; (*d*) line average electron density and divertor D_α emission, indicating ELM timing and (*e*) injected neutral beam power. (Colour online.)

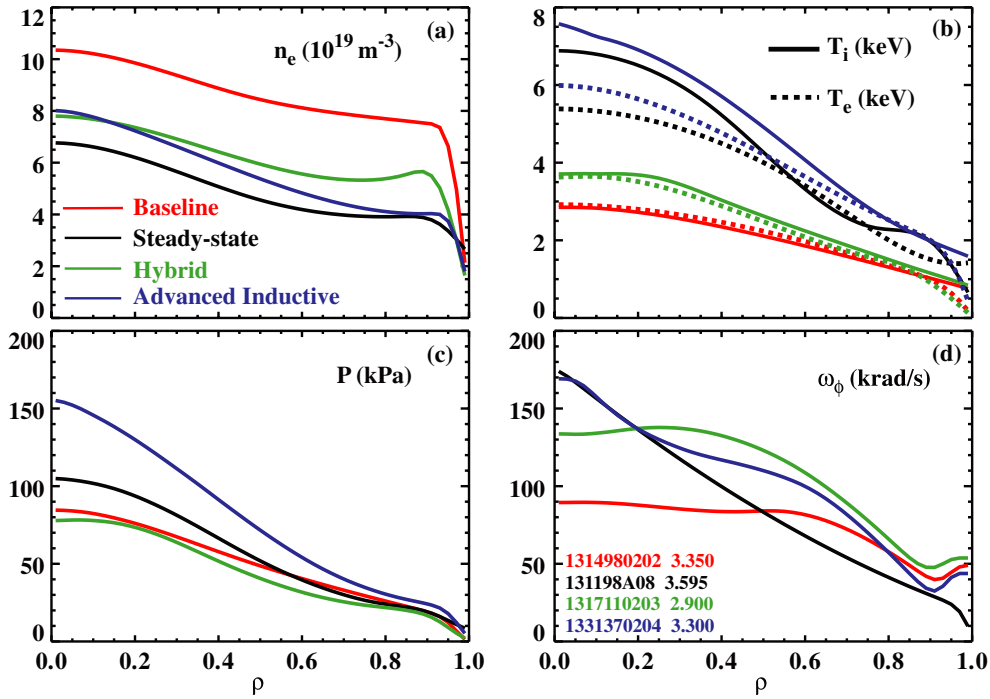

Figure 3. Profiles as a function of normalized radius ρ for (a) electron density n_e, (b) ion and electron temperatures T_i and T_e, (c) plasma pressure P and (d) plasma rotation ω_φ, for baseline (131498, in red), steady-state (131198, in black), hybrid (131711, in green) and AI (133137, in blue) scenario plasmas. Note that all four discharges shown were operated at a common field of 1.9 T, such that the plasma pressures can be directly compared. The advanced scenarios have the same pressure as the baseline scenario at lower I_p or higher pressure at equal I_p.

Profiles for the baseline scenario, figure 3, show that $T_e \sim T_i$ across the plasma radius, as might be expected at such operating densities. The density profile is substantially peaked, as opposed to the flat density profile assumed in standard ITER profile models [19], but in qualitative agreement with recent AUG and JET observations and predictions of peaked density profiles [20]. Plasma rotation is significant in the baseline and other scenarios, (see figure 3(d), and values in table 1), due to the all co-neutral beam injection used in these discharges. DIII-D has a counter-neutral beam injection capability, which would enable operation at the same target β_N, but with lower net torque, but this was not attempted in these experiments. No firm predictions exist for plasma rotation on ITER [10], though it is expected that rotation will be low compared with the discharges reported here, as a consequence of higher NBI voltage and lower momentum input. The ion and electron thermal transport rates have been calculated using the TRANSP code [21], and indicates that ion transport is above neoclassical.

The L–H transition in the baseline scenario discharges, figure 4, is triggered shortly after the application of a fixed NBI power of ~4.4 MW, which exceeds the threshold power (P_{th}) as predicted by the latest scaling relation [22]. A separate discharge with fixed input NBI power of 2.6 MW and a density of 4.0×10^{19} m^{-3} remained in L-mode for over a second with a ratio of the loss power (P_L) to P_{th} of ~2, until an L–H transition was eventually triggered by a sawtooth, indicating a power threshold approximately a factor of two higher than the scaling prediction for DIII-D with this plasma shape. After the L–H transition, with the NBI under feedback control to maintain $\beta_N = 1.8$, the P_L/P_{th} ratio declines as the density

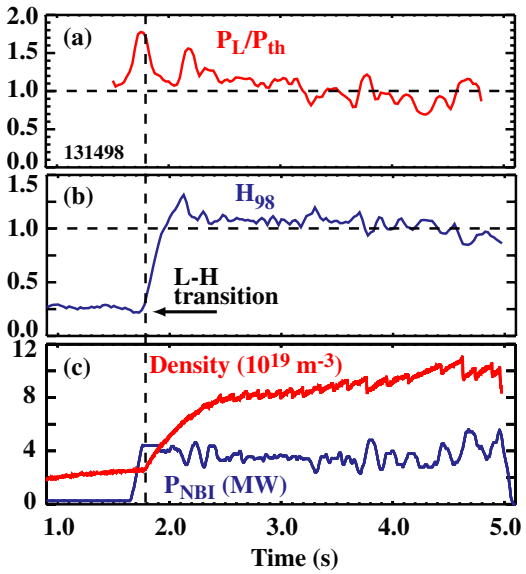

Figure 4. Time evolution of (a) ratio of loss power to calculated L–H transition power, (b) confinement factor H_{98} and (c) line density and injected neutral beam power for baseline scenario discharge 131498. A shorter time average is used for the line density data here as compared with the same data in figure 2(d), such that the effect of individual ELMs on the density can be more clearly distinguished. (Colour online.)

rises (figure 4(a)), down to ~0.8, and some of the discharges exhibit H–L back-transitions. (Note that this use of the scaling law to calculate a P_{th} during the H-mode period is questionable, as the scaling was derived specifically for the L–H transition, not the H–L back-transition.)

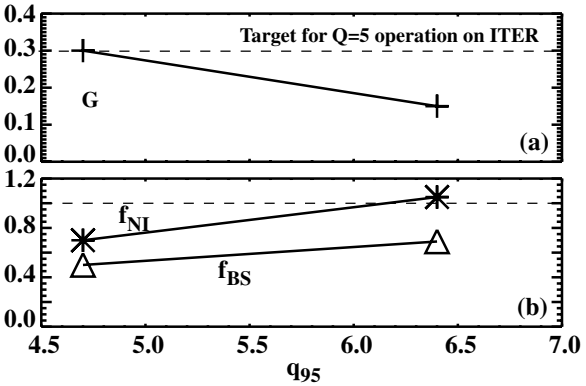

Figure 5. Variation of (*a*) fusion gain parameter G and (*b*) NI and bootstrap current fractions with q_{95} in steady-state demonstration discharges.

4. ITER steady-state scenario

Steady-state demonstration discharges were operated using a standard DIII-D prescription [23, 24], with early neutral beam heating to induce an L–H transition during the current-ramp phase. Off-axis current drive was provided by up to 3 MW of ECCD, using a relatively broad deposition profile, covering ρ of ~0.3–0.6, to provide improved 2/1 NTM stability [23]. The discharges were operated over a range of plasma currents, corresponding to 8.5–10.8 MA operation on ITER, and q_{95} of 4.7–6.3, with an elevated q-profile, $q_{\min} \geqslant 1.5$. At the lowest currents, full NI or overdriven operation was obtained, but with relatively low fusion performance. Conversely, at the highest current, the discharges were not fully NI, but had fusion performance at the $G \sim 0.3$ level predicted for $Q \sim 5$ operation on ITER. This trade-off between fusion performance and steady-state capability is illustrated in figure 5. Simultaneously meeting the ITER goals for fusion performance and steady-state operation requires higher β_N at the higher currents, so as to supply additional bootstrap current.

The time evolution of the main plasma parameters for an 8.5 MA equivalent discharge is illustrated in figure 6, while profiles are shown in figure 3, to facilitate comparison with the baseline scenario. The surface loop voltage for this discharge is ±5 mV (figure 6(*d*)), consistent with full NI operation, while TRANSP analysis indicates overdrive after ~3 s. As compared with the baseline discharges, the lower densities associated with steady-state operation result in $T_i > T_e$ inside $\rho = 0.5$, see figure 3(*b*). All discharges shown in figure 3 were operated at 1.9 T, such that the plasma pressures can be directly compared. The advanced steady-state scenario, at lower I_p, achieved comparable values of β_T as in the baseline scenario at higher I_p. As shown in figure 6(*b*), confinement is at the conventional level for ELMing H-mode, with $H_{98} \sim 1.0$. The data illustrated in table 1 are for one of the higher current (10.7 MA equivalent), higher fusion performance discharges.

Matching the ITER plasma cross-section and aspect ratio, while maintaining a pumping capability on DIII-D, results in the scaled ITER shape shown in figure 1, which has a large, ~13 cm, plasma–wall gap (i.e. plasma to first tile gap) at the outboard midplane. With this large gap the maximum sustained β_N which could be operated was ~2.8. This value of β_N barely exceeds the ideal MHD $n = 1$ no-wall limit

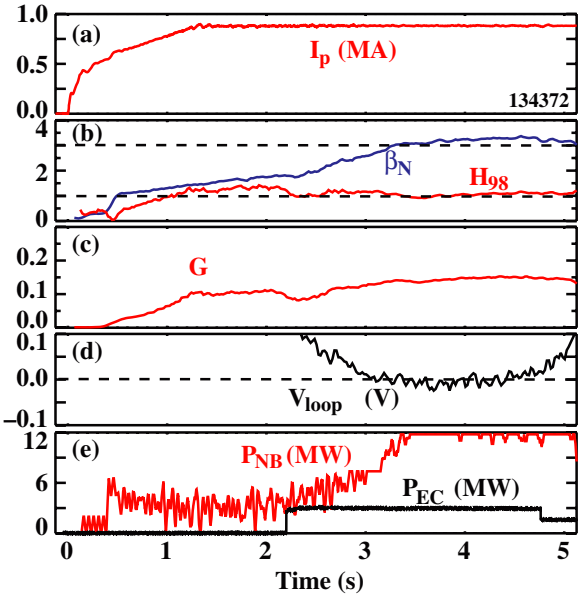

Figure 6. Time evolution of key plasma parameters for a steady-state scenario demonstration discharge, operating at a normalized plasma current equivalent to 8.5 MA on ITER (134372). Illustrated are (*a*) plasma current I_p, (*b*) normalized beta β_N and confinement factor H_{98}, (*c*) fusion performance factor G, (*d*) surface loop voltage V_{loop} and (*e*) injected neutral beam and ECCD powers. (Colour online.)

as calculated with the DCON code [25]. At larger values of β_N, which can be accessed transiently, the amplification of an externally applied slowly rotating $n = 1$ field rapidly increases, indicating a significant reduction in the stability of the $n = 1$ resistive wall mode [26]. However, by operating the discharges with a smaller size scaling factor of 3.48 (as opposed to 3.7), the outer gap was reduced to ~8.5 cm, a more typical value for DIII-D AT discharges. With this reduced gap, wall stabilization was apparently increased, and sustained plasma operation was achieved with β_N of 3.1–3.3, as shown in figure 6. This change in achievable β_N was not due to variation in the no-wall limit, as shown by measurements of the $n = 1$ field amplitude, figure 7. The steady-state discharge listed in table 1 (131198) had the larger outer gap, similar to the other scenarios.

5. Hybrid scenario

Using the standard DIII-D prescription for hybrid operation [4], a limited number of discharges were operated at a current equivalent to 11.4 MA on ITER, with $q_{95} = 4.3$. These discharges had a maximum sustained β_N of ~2.2, substantially less than normal for DIII-D hybrid plasmas [5]. However, discharges run with the ITER 'large-bore' startup prescription, with no heating during the current-ramp phase and a slightly modified (less-realistic) version of the ITER shape, exhibited substantially higher performance. These discharges, with a current equivalent to 11.2 MA on ITER, $q_{95} = 4.1$ and $B_T = 2.1$ T, are described in detail in a companion paper [13]. An example of an ITER-like startup hybrid scenario discharge is shown in figure 8, demonstrating sustained operation with $\beta_N = 2.8$ and excellent confinement, $H_{98} = 1.45$, comfortably

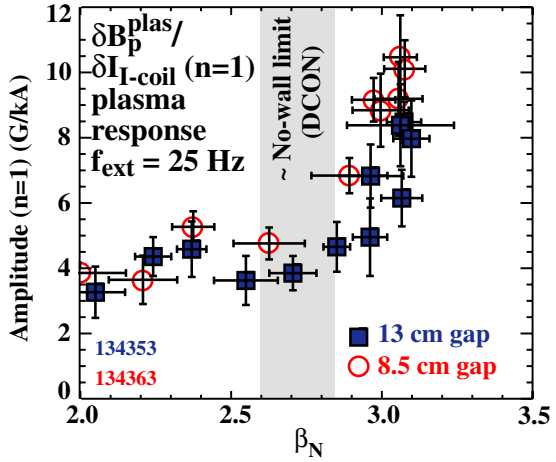

Figure 7. Measurements of the amplitude of the plasma poloidal magnetic field response, $\delta B_{\rm p}^{\rm plas}$, to an externally applied $n = 1$ field, normalized by the current in non-axisymmetric coils, $\delta I_{\rm I-coil}$, as a function of $\beta_{\rm N}$, for steady-state plasmas with 13 cm and 8.5 cm outer gap plasmas (shown in squares and open circles, respectively). A rapid increase in the plasma response indicates proximity to the no-wall limit, which occurs at approximately the same $\beta_{\rm N}$ in both cases. (Colour online.)

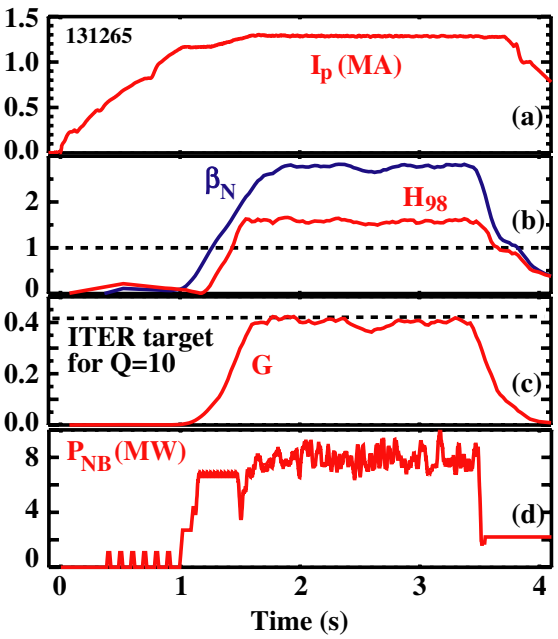

Figure 8. Time evolution of key plasma parameters for a hybrid scenario demonstration discharge, operating at a normalized plasma current equivalent to 11.2 MA on ITER (131265). This discharge had an ITER-like startup phase, and was operated with $B_{\rm T}$ of 2.1 T. Shown are (a) plasma current $I_{\rm p}$, (b) normalized beta $\beta_{\rm N}$ and confinement factor H_{98}, (c) fusion performance factor G, with target value for $Q = 10$ operation on ITER indicated and (d) injected neutral beam power. (Colour online.)

exceeding the ITER targets [1] of 2.0–2.5 and 1.0–1.2, respectively. By contrast, the profiles shown in figure 3 are from one of the DIII-D-like startup hybrid plasmas, as this has the same $B_{\rm T}$ of 1.9 T used for the other scenarios. As compared with the baseline scenario, the hybrids operate at lower density, with higher rotation and $T_{\rm i}$ somewhat higher

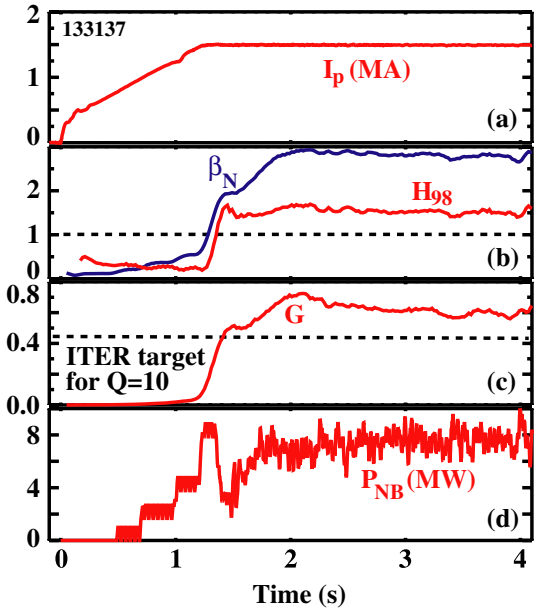

Figure 9. Time evolution of key plasma parameters for AI scenario demonstration discharge, operating at a normalized plasma current equivalent to 14.8 MA on ITER (133137). Illustrated are (a) plasma current $I_{\rm p}$, (b) normalized beta $\beta_{\rm N}$ and confinement factor H_{98}, (c) fusion performance factor G, with target value for $Q = 10$ operation on ITER indicated and (d) injected neutral beam power. (Colour online.)

than $T_{\rm e}$. Summary details for hybrid discharges with a DIII-D-like startup (131711) and an ITER-like startup (131265) are included in table 1. As can be seen, in addition to addressing the ITER hybrid mission, these discharges also offer a possible alternative route to achieving the ITER $Q = 10$ mission, but at reduced current.

6. AI scenario

These discharges utilized the standard DIII-D prescription for hybrid operation [4, 5], but at higher current, equivalent to 14.8 MA on ITER, with $q_{95} = 3.3$. As shown in figure 9, this combination resulted in a discharge exhibiting very high fusion performance, with $\beta_{\rm N} = 2.8$, $H_{98} = 1.5$ and $G = 0.6$. As compared with the baseline scenario, ELMs are more frequent and smaller, giving good density control. Profiles for this discharge are included in figure 3, where they can be compared with those of the other scenarios. Again, for the data shown in figure 3, all discharges were operated at a common field of 1.9 T, allowing the plasma pressures to be directly compared, and showing that the AI scenario achieves substantially higher plasma pressure than the baseline scenario, at equivalent $I_{\rm p}$. As seen in table 1, this discharge projects to very high performance on ITER, with >700 MW of fusion power and Q of $\sim 13 - \infty$, depending on the confinement scaling utilized.

7. ITER physics issues illustrated by the demonstration discharges

A major benefit of the demonstration discharges is that they address many of the leading physics issues facing

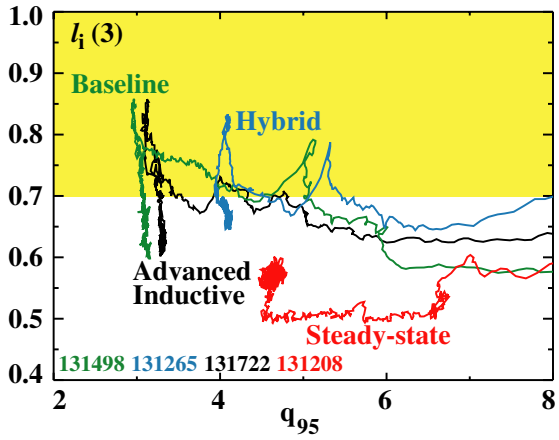

Figure 10. Trajectories in $l_i(3)$ versus q_{95} space for each operating scenario. The discharges all begin at the right-hand side with high q_{95} and progress to the left. The yellow shaded region indicates the original ITER design range in $l_i(3)$ for 15 MA operation.

ITER. Among such issues encountered in the demonstration discharges are the L–H transition power threshold (discussed earlier in section 3), the size and impact of ELMs, pedestal parameter scaling, the impact of tearing modes on confinement and disruptivity, beta limits and the required capabilities of the plasma control system. One area where the demonstration discharges have already had a significant impact on the ITER design is with regard to the physics requirements on the poloidal field coil system. ITER was originally designed for plasma internal inductances in the range 0.7–1.0 at 15 MA (ITER employs $l_i(3)$ as a measure of internal inductance, see [13]). However, as shown in figure 10, the measured values for $l_i(3)$ for all four scenarios evolve during the plasma flat-top phase to values below 0.7, with some values as low as 0.5 (though two of these regimes have plasma current below the 15 MA level at which the control range was specified). Having $l_i(3)$ values outside the ITER design range would result in a loss of plasma shape control on ITER. In response to these results from DIII-D, and other devices [27], the operating range of the ITER shape control system is being expanded [28].

Another key issue for ITER is that of achieving tolerable ELM characteristics. As part of the ITER design update process, the allowable limits for energy loss per ELM (ΔW_{ELM}) are being reduced to $\leqslant$1 MJ or $\leqslant$1% of the pedestal energy [29]. The impact of individual ELMs on the plasma total stored energy and density in a DIII-D baseline scenario discharge is shown in detail in figure 11. As can be seen, each ELM causes a loss of ~15% of the total stored energy, and ~30% of the pedestal energy. This observed ΔW_{ELM} substantially exceeds the allowable ITER limits [29]. As shown in figure 12, this energy loss/ELM in the baseline scenario is also well above the standard scaling for ELM energy loss [30], indicating the critical need for a robust ELM suppression system on ITER. The fact that these ELMs exceed the standard scaling is probably associated with their very large radial extent, into $\rho \sim 0.5$ in the plasma pressure profile. Modelling with the ELITE code [31] is consistent with type I ELM behaviour governed by intermediate-n peeling ballooning stability, but with a wider radial eigenmode extent than usual. Figure 12 also shows that the energy loss/ELM observed in the other

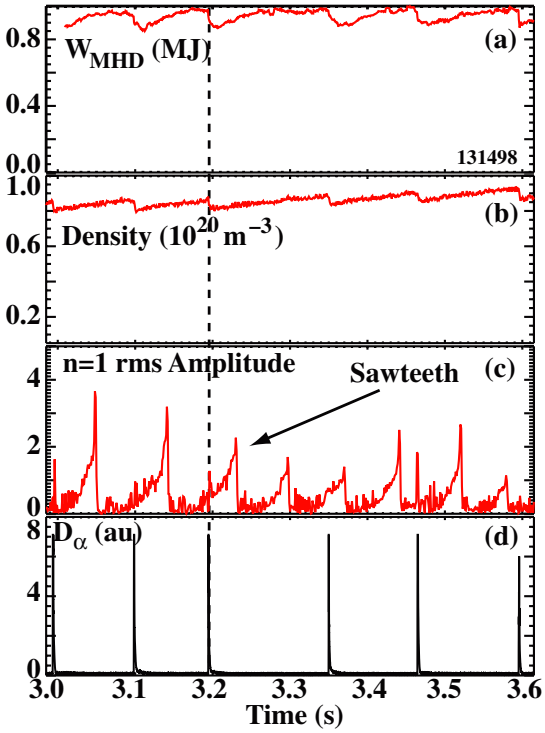

Figure 11. Total stored energy and density variations induced by individual type I ELMs in the baseline scenario discharge shown in figure 2 (131498). Illustrated are (*a*) total stored energy, (*b*) electron line density, (*c*) rms amplitude of an instability with toroidal mode number $n = 1$, associated with sawtooth activity and (*d*) divertor D_α emission, indicating ELM timing. The ELMs and sawteeth are out of phase. (Colour online.)

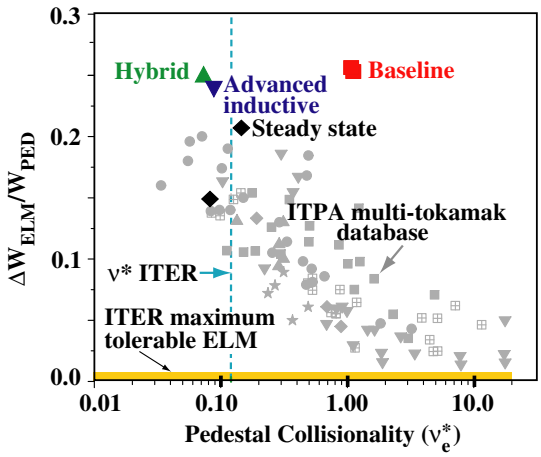

Figure 12. Fractional energy loss per ELM versus pedestal collisionality for the four ITER scenarios. The background data from the ITPA multi-tokamak database are from [30]. (Colour online.)

three scenarios is in-line with the standard scaling. The measured pedestal conditions in these ITER scenario plasmas are also being used as part of the experimental tests [32] of a new predictive model for the pedestal height, EPED1 [33]. Illustrated in figure 13 is a comparison of the measured and predicted edge pedestal heights for the baseline, hybrid and AI scenarios, showing good agreement between the measurements and the EPED1 model [32, 33].

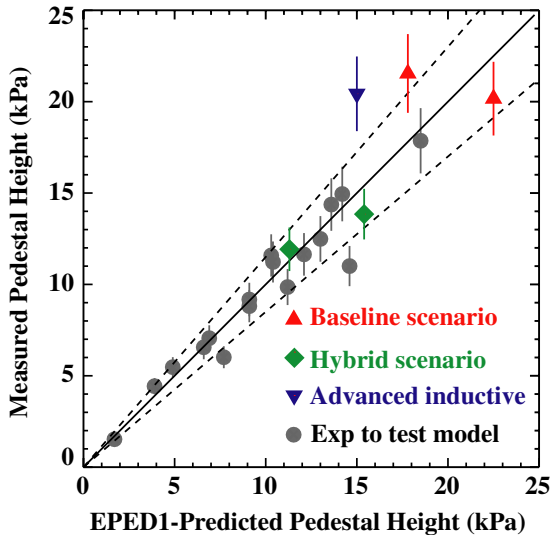

Figure 13. Measured H-mode edge pedestals heights versus EPED1 model predictions for the pedestal height for the baseline, hybrid and AI ITER scenarios, showing excellent agreement. (Colour online.)

8. Conclusions

Four leading ITER operational scenarios have been successfully demonstrated on DIII-D, namely the baseline, hybrid, AI and steady-state scenarios. The DIII-D plasmas incorporate essential features of the ITER scenarios and their anticipated operating characteristics, such as the plasma cross-section (with size reduced by a factor of 3.7), aspect ratio and target values for β_N, H_{98} and I/aB. The results of these demonstrations are uniformly positive with regard to ITER meeting its performance targets for fusion gain (Q) and fusion power production. The DIII-D discharges project to a fusion power output in the range of ~400–800 MW, with Q of ~5 to infinity, depending on scenario and confinement scaling utilized. Of course, the DIII-D discharges did not match all anticipated ITER conditions, and thus the projections have to be treated with care. In particular, the DIII-D baseline scenario discharges operated with a lower Greenwald density fraction and at higher plasma rotation than anticipated for ITER, both factors which are known to affect confinement and transport and hence fusion performance. The demonstration discharges also provide crucial information on many of the key physics issues facing ITER, such as ELM behaviour and pedestal scaling, where the observations support the critical need for a robust ELM suppression system on ITER. The DIII-D results have also directly influenced the evolution of the ITER design, having indicated the need for a broader operating range in internal inductance for the poloidal field coil set.

Acknowledgment

This work was supported in part by the US Department of Energy under DE-FG03-01ER54615, DE-AC02-76CH03073, DE-FC02-04ER54698, DE-FG02-95ER54309, DE-AC05-00OR22725, DE-FG02-89ER53297, DE-AC52-07NA27344 and DE-FG02-89ER53296.

References

[1] Shimada M. *et al* 2007 Progress in the ITER Physics Basis, Chapter 1: Overview and summary *Nucl. Fusion* **47** S1
[2] Cordey J.G. *et al* 1996 *Plasma Phys. Control. Fusion* **38** 1237
[3] Kamada Y. and the JT-60 Team 2001 *Nucl. Fusion* **41** 1311
[4] Luce T.C., Wade M.R., Ferron J.R., Politzer P.A., Hyatt A.W., Sips A.C.C. and Murakami M. 2004 *Phys. Plasmas* **11** 2627
[5] Wade M.R. *et al* 2005 *Nucl. Fusion* **45** 407
[6] Joffrin E. *et al* 2005 *Nucl. Fusion* **45** 626
[7] Gormezano C. *et al* 2007 Progress in the ITER Physics Basis, Chapter 6: Steady State Operation *Nucl. Fusion* **47** S285
[8] Ferron J.R. *et al* 2005 *Phys. Plasmas* **12** 056126
[9] Gates D.A. *et al* 2006 *Phys. Plasmas* **13** 056122
[10] Doyle E.J. *et al* 2007 Progress in the ITER Physics Basis, Chapter 2: Plasma confinement and transport *Nucl. Fusion* **47** S02
[11] Leonard A.W., Groebner R.J., Osborne T.H. and Snyder P.B. 2008 *Phys. Plasmas* **15** 056114
[12] Jackson G.L. *et al* 2008 *Nucl. Fusion* **48** 125002
[13] Jackson G.L., Casper T.A., Luce T.C., Humphreys D.A., Ferron J.R., Hyatt A.W., Leuer J.A., Petrie T.W., Turco F and West W.P. 2009 *Nucl. Fusion* **49** 115027
[14] Politzer P.A. *et al* 2008 *Nucl. Fusion* **48** 075001
[15] Yushmanov P.N., Takizuka T., Reidel K.S., Kardoun O.J.W.E., Corley J.G., Kaye S.M. and Post D.E. 1990 *Nucl. Fusion* **30** 1999
[16] Petty C.C., DeBoo J.C., La Haye R.J., Luce T.C., Politzer P.A. and Wong C.P.C. 2003 *Fusion Sci. Technol.* **43** 1
[17] ITER Physics Expert Group on Confinement, Transport, ITER Physics Expert Group on Confinement Modelling, Database, and ITER Physics Basis Editors 1999 Chapter 2: Plasma confinement and transport *Nucl. Fusion* **39** 302
[18] La Haye R.J., Isayama A. and Maraschek M. 2009 *Nucl. Fusion* **49** 045005
[19] Polevoi A.R., Shimada M., Sugihara M., Igitkhanov Yu.L., Mukhovatov V.S., Kukushkin A.S., Medvedev S.Yu., Zvonkov A.V. and Ivanov A.A. 2005 *Nucl. Fusion* **45** 1451
[20] Angioni C. *et al* 2007 *Phys. Plasmas* **14** 055905
[21] Hawryluk R.J. 1980 *Proc. Course in Physics Close to Thermonuclear Conditions (Varenna, Italy, 1979)* vol 1 (Brussels: CEC) p 19
[22] Martin Y.R., Takizuka T and ITPA CDBM H-mode Threshold Database Working Group 2008 *J. Phys: Conf. Ser.* **123** 012033
[23] Murakami M. *et al* 2006 *Phys. Plasmas* **13** 056106
[24] Ferron J.R. *et al Proc. 22nd Int. Conf. on Fusion Energy 2008 (Geneva, Switzerland, 2008)* (Vienna: IAEA) CD-Rom file EX/P4-27 and http://www-naweb.iaea.org/napc/physics/FEC/FEC2008/html/index.htm
[25] Glasser A. and Chance M.S. 1997 *Bull. Am. Phys. Soc.* **42** 1848
[26] Reimerdes H., Chu M.S., Garofalo A.M., Jackson G.L., La Haye R.J., Navratil G.A., Okabayashi M., Scoville J.T. and Strait E.J. 2004 *Phys. Rev. Lett.* **93** 135002
[27] Sips A.C.C. *et al* 2009 *Nucl. Fusion* **49** 085015
[28] Hawryluk R.J. *et al* 2009 *Nucl. Fusion* **49** 065012
[29] Loarte A. *et al* 2008 *Proc. 22nd Int. Conf. on Fusion Energy 2008 (Geneva, Switzerland, 2008)* (Vienna: IAEA) CD-Rom file IT/P6-13 and http://www-naweb.iaea.org/napc/physics/FEC/FEC2008/html/index.htm
[30] Loarte A. *et al* 2003 *J. Nucl. Mater.* **313–316** 962
[31] Snyder P.B., Wilson H.R., Ferron J.R., Lao L.L., Leonard A.W., Osborne T.H., Turnbull A.D., Mossessian D., Murakami M. and Xu X.Q. 2002 *Phys. Plasmas* **9** 2037
[32] Groebner R.J., Leonard A.W., Snyder P.B., Osborne T.H., Maggi C.F., Fenstermacher M.E., Petty C.C. and Owen L.W. 2009 *Nucl. Fusion* **49** 085037
[33] Snyder P.B. *et al* 2009 *Nucl. Fusion* **49** 085035